



Surface defect passivation by 1,8-Naphthyridine for efficient and stable Formamidinium-based 2D/3D perovskite solar cells

Guodong Li¹, Jing Song¹, Jihuai Wu^{*}, Yuan Xu, Chunyan Deng, Zeyu Song, Xiaobing Wang, Yitian Du, Qi Chen, Ruoshui Li, Weihai Sun, Zhang Lan^{*}

Engineering Research Center of Environment-Friendly Functional Materials, Ministry of Education, Institute of Materials Physical Chemistry, Huaqiao University, Xiamen 361021, China



ARTICLE INFO

Keywords:
Perovskite solar cells
1,8-Naphthyridine
Surface defect
2D/3D
 α -FAPbI₃

ABSTRACT

The ionic properties of components determine that perovskite films will generate numerous charged surface defect under continuous high-temperature annealing, resulting in suboptimal performance and poor stability of perovskite solar cells (PSCs). Based on the principle of Lewis acid-base coordination, 1,8-naphthyridine (1,8-ND) with electron-rich structure was used to form complexes with Pb²⁺ ions, and high-quality 2D/3D perovskite films with effective defect passivation were prepared by surface modification. Benefiting from suppressed nonradiative recombination, extended carrier lifetime, modified charge transport, improved hydrophobic properties and the optimized phase stability of α -FAPbI₃, 1,8-ND modified 2D/3D PSCs with negligible hysteresis and satisfactory stability achieved a champion power conversion efficiency of 23.8% whose open circuit voltage was significantly improved from 1.09 V to 1.15 V, providing a resultful strategy to passivate surface defect while constructing 2D/3D perovskite.

1. Introduction

Perovskite solar cells (PSCs) have aroused strong repercussions in photovoltaic field due to their unique and excellent properties [1–3]. Recently, based on the regulation of perovskite components and the optimization of carrier transport materials, the power conversion efficiency (PCE) of PSCs has surged from 3.8% to the latest internationally certified 25.7%, which is rivalrous to mature silicon based photovoltaic technology, meets the efficiency requirement of commercialization, with broad application prospects [4–6].

FAPbI₃ perovskite based on the organic cation of formamidine (FA) has a suitable band gap, which can ensure the absorption of incident light and improve the current output of prepared PSCs. With excellent the absorption property of light and outstanding thermal and light stability, FAPbI₃ has begun to show its potential and has become the current mainstream light absorbing material [7,8]. However, FAPbI₃ generally requires relatively small-sized methylamine (MA) cations to stabilize its photoactive α -phase, and MAI is usually introduced to control the crystallization of perovskite films [9–11]. Moreover, the crystallization of perovskite films with ionic property requires

continuous high-temperature annealing. At the same time, the ionic components in perovskite will volatilize and segregate on crystal surface, resulting in the generation of numerous halogen vacancies, organic cation vacancies, anti-sites, uncoordinated Pb²⁺ ions and metal Pb clusters [12,13]. Defect at grain boundary and surface will adversely affect the transport of carriers, cause non-radiative recombination, aggravate open circuit voltage (V_{OC}) loss, trigger degradation of perovskite, affect stability of PSCs, and seriously damage optoelectronic properties of prepared PSCs [14]. Optimizing the crystallization of perovskite films based on introducing additives or improving preparation process is an effective strategy to control defect generation, leading to a conspicuous improvement in the performance of prepared PSCs [15,16]. However, surface defect of perovskite films has been reported to be two to four orders of magnitude higher than bulk defect [17]. Therefore, it is particularly urgent to design a passivation strategy for reducing surface defect. It has been reported that undercoordinated Pb²⁺ due to continuous annealing will exhibit Lewis acid property [18]. Lewis base molecules can passivate Pb²⁺ defect by donating or sharing electron pairs and forming Lewis acid-base adduct, thereby reducing the loss of photogenerated carriers, enhancing the photoelectric property

* Corresponding authors.

E-mail addresses: jhwu@hqu.edu.cn (J. Wu), lanzhang@hqu.edu.cn (Z. Lan).

¹ These authors contributed equally to this work.

and improving the stability of PSCs [19–21]. In addition, two-dimensional (2D) perovskite has been identified to inhibit the penetration of moisture, limit the migration of ions, stabilize α -FAPbI₃ phase, and ultimately improve the aging stability of PSCs [22,23]. However, exciton binding energy of 2D perovskite is extremely large, which seriously affects its light absorption [24]. Thus, 2D/3D perovskite integrating high PCE of 3D perovskite and outstanding stability of 2D perovskites has attracted extensive attention and has promising prospect [25,26].

In this work, we employed 1,8-Naphthyridine (1,8-ND) as an interfacial modification material between perovskite/HTL (hole transport layer) films to fabricate efficient and stable 2D/3D PSCs with effective surface defect passivation. The results showed that the electron-rich 1,8-ND molecules can form effective coordination with Pb²⁺ ions and construct structurally stable 2D/3D perovskite films. The optimized perovskite films had reduced defect density, extended carrier lifetime, excellent hydrophobic properties and better stability of α -FAPbI₃ phase. Finally, the PSCs modified with 1,8-ND at surface achieved a champion PCE of 23.8% and an excellent environmental stability.

2. Results and discussion

The nucleation and growth of perovskite crystal depend on volatilization of precursor solvent and continuous high-temperature annealing,

resulting in abundant defect at grain boundary and surface of perovskite films [27]. Moreover, the growth of crystal will be terminated at surface, and upper surface of perovskite films is contact with external environment in direct, which results in the surface between perovskite/HTL films becoming a defect-rich site, heavily limits the performance of PSCs [12]. We prepared FA-based perovskite (FA_{0.92}MA_{0.08}PbI₃) films by a traditional two-step process, and then coated the upper surface of the annealed perovskite film with 1,8-naphthyridine (1,8-ND) dissolved in isopropanol for modification. The corresponding experimental procedures can be found in the [Supplementary Materials](#).

The fitted electron cloud distribution of 1,8-Naphthyridine (1,8-ND) as a representative Lewis base is shown in Fig. 1a. The electron cloud distribution on two nitrogen (N) atoms is equal, which can evenly donate non-bonding electrons. In addition, p- π conjugated structure ensures the electrical conductivity. Therefore, we depict a schematic diagram shown in Fig. 1b. When 1,8-ND is deposited in situ between perovskite/HTL films as a modification material, its Lewis base property can clamp exposed Pb²⁺ or Pb clusters which is locked at surface or grain boundary by donating uncoordinated electrons to the vacant 6p orbital of Pb²⁺ ions, playing a role in passivating Pb defect [28,29]. In addition, along with coordination of N atoms with perovskite, its thiffer hydrophobic ring can effectively inhibit the penetration of H₂O molecules, thereby optimizing the moisture resistance of perovskite films and ultimately improving the humidity stability of PSCs.

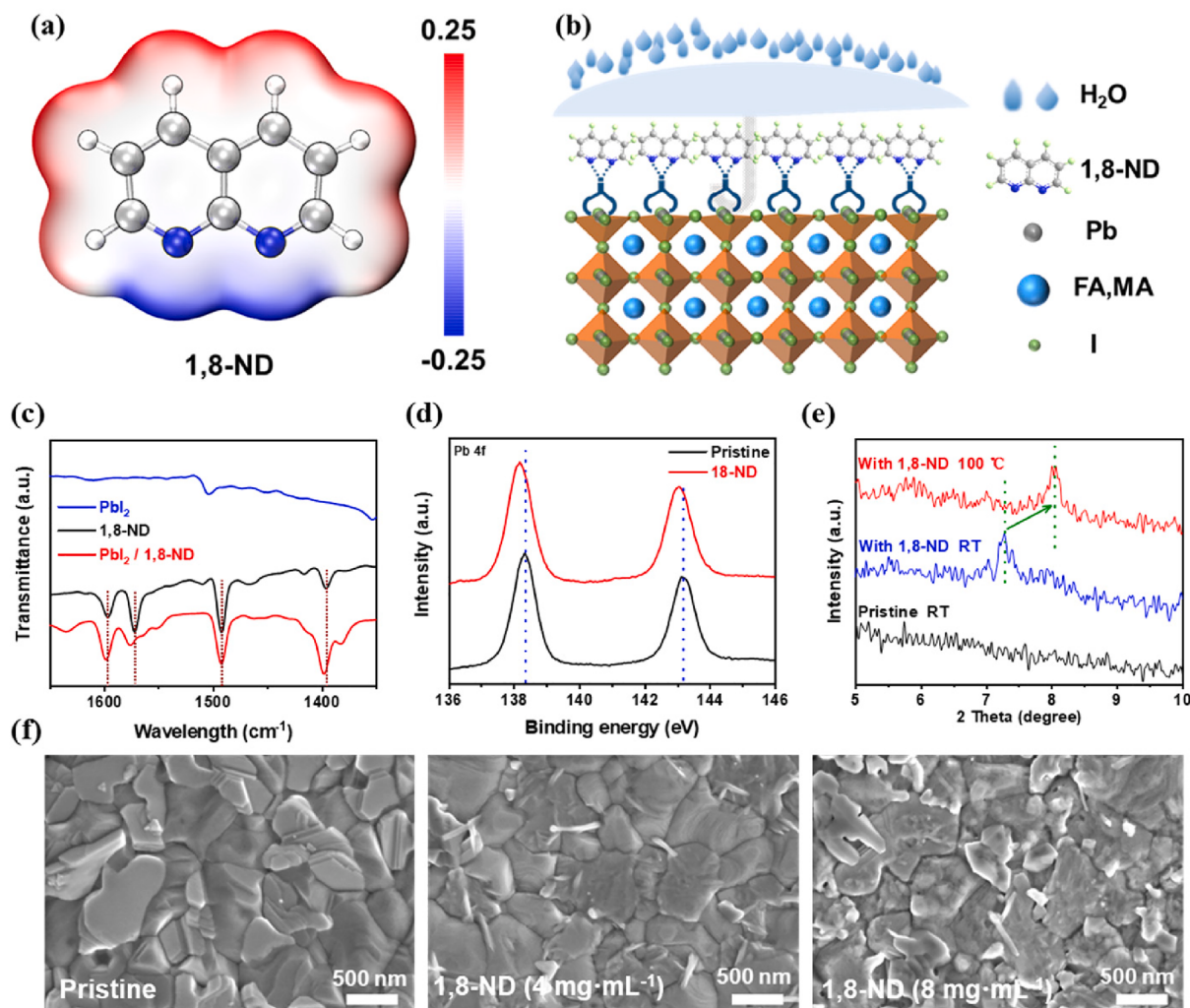


Fig. 1. (a) Electrostatic surface potential (ESP) map of 1,8-ND molecule (red indicates electronegative part and blue indicates electropositive part). (b) Schematic diagram of modified perovskite by 1,8-ND molecules. (c) FTIR spectra of films of PbI₂, 1,8-ND and PbI₂ covered with 1,8-ND. (d) XPS spectra (Pb 4f), (e) XRD patterns (RT and 100 °C indicate room temperature and 100 °C annealing treatment), (f) Top-view SEM images of pristine and 1,8-ND modified perovskite films.

In order to verify that 1,8-ND can coordinate with Pb^{2+} , Fourier transform infrared (FTIR) spectrometer was performed on 1,8-ND film, PbI_2 film and the film deposited with 1,8-ND on PbI_2 . As shown in Fig. 1c, the $\text{C}_{\text{ar}} = \text{C}_{\text{ar}}$ and $\text{C}_{\text{ar}} = \text{N}$ stretching vibration signals of 1,8-ND located at 1396, 1572 and 1597 cm^{-1} are shifted to 1398, 1576 and 1599 cm^{-1} after binding to PbI_2 , which indicates the interaction between Pb^{2+} and conjugated N atoms in 1,8-ND molecules [30]. It is worth noting that the symmetrical two N atoms can form a bidentate chelate with Pb^{2+} , thereby passivating uncoordinated Pb^{2+} more efficiently [31]. In order to further clarify the bonding situation between 1,8-ND and perovskite components, X-ray photoelectron spectroscopy (XPS) of perovskite films were compared and analyzed (Fig. S1a). It can be seen from Pb 4f spectra in Fig. 1d that the two characteristic peaks corresponding to 138.3 eV (Pb 4f_{7/2}) and 143.2 eV (Pb 4f_{5/2}) are shifted towards lower binding energy direction, which is the result of increased electron cloud density around Pb^{2+} on perovskite film surface, indicating that 1,8-ND molecules can form effective coordination with Pb^{2+} [32]. It can be judged from C 1 s spectra of Fig. S1b that the characteristic peak of C = N in FA located at 288.2 eV shifts to the direction of lower binding energy. This may be on account of the donated electrons of 1,8-ND molecules, which increases the density of electron clouds around FA^+ , resulting in the formation of hydrogen bonds between 1,8-ND molecules and FA^+ [33]. In addition, an additional peak at 399.2 eV can be observed for 1,8-ND modified perovskite film in N 1 s spectra of Fig. S1c, which may be owe to the conjugated C – N – C bond of naphthyridine ring [34]. Meanwhile, the shift of C – N bond located at 400.4 eV further suggested that 1,8-ND molecule might form hydrogen bond with FA^+ [34]. Fig. S1d further demonstrates the electron-donating property of 1,8-ND molecule through the shift of I 3d characteristic peaks.

In order to judge whether the perovskite crystal structure had changed, X-ray diffraction (XRD) analysis of prepared perovskite films was carried out. As shown in Fig. S2a, 1,8-ND modified perovskite film reveals a new characteristic peak at $2\theta = 8.1^\circ$ after 100 °C annealing, which is the same as the position after deposition of 1,8-ND on PbI_2 film shown in Fig. S2b, but different from that of 1,8-ND in Fig. S2c. According to the Bragg equation of X-ray diffraction, new characteristic peaks appear at small-angles when 2D perovskite diffracts with wider interplanar spacing [32]. The new diffraction peaks illustrate that 1,8-ND can trigger the formation of 2D perovskite due to its unique configuration, which is beneficial for film to resist the erosion of H_2O molecules [35]. Notably, pyridine with less steric hindrance cannot construct 2D perovskite according to the previous report [36]. To further verify the formation of quasi-2D perovskite, transmission electron microscope (TEM) image was measured and shown in Fig. S2d. 1,8-ND modified perovskite has a 11.2 Å interplanar spacing, which is consistent with the XRD results. Moreover, it can be found that after the films were annealed at 100 °C, the characteristic peaks at low angle shifted from 7.2° to 8.1°. Local XRD patterns (Fig. 1e) can more clearly judge the shift of low angle characteristic peaks after annealing. Obviously, this is the result of the reduction in corresponding interplanar spacing, which may be on account of 1,8-ND molecules between inorganic layers tend to be staggered arrangement under annealing treatment (Fig. S2e), thereby reducing the interplanar spacing of 2D perovskite [16,37].

The effect of 1,8-ND surface modification can be judged more intuitively based on the analysis of morphology on perovskite films by top-view scanning electron microscopy (SEM). It can be seen from Fig. 1f that there are more incompletely reacted sheet-like PbI_2 on the upper surface of pristine perovskite film, which is inseparable from continuous high temperature annealing and faster crystal growth rate of perovskite, consistent with XRD results [9]. After 1,8-ND modification, unchanged perovskite particle size indicates that no recrystallization process occurred. However, the surface morphology of perovskite grains, especially PbI_2 , changed significantly, which may be due to the formation of quasi-2D perovskite by 1,8-ND. Moreover, the sheet-like PbI_2 on the 1,8-

ND modified film is also reduced compared to the pristine perovskite film. After the modification concentration of 1,8-ND continued to increase, the change of surface morphology became more obvious. It can be speculated that the dramatic change in morphology may be concerned with the formation of quasi-2D perovskite [31,38]. In addition, it can be seen from the atomic force microscopy (AFM) images in Fig. S3 that there are more sheet-like PbI_2 on the surface of pristine perovskite film, while the surface morphology of 1,8-ND modified perovskite film has changed significantly, which is consistent with SEM results.

Ultraviolet-visible absorption (UV-vis) spectra can further indicate the effect of 1,8-ND on perovskite crystal quality. Fig. 2a display that 1,8-ND modified perovskite film has better light absorption, especially in the wavelength less than 600 nm, the enhancement of absorption is more obvious. Therefore, optimized perovskite films will generate more photogenerated carriers under illumination, which in turn effectively increases the output current of prepared PSCs. In addition, coincide absorbing edges means that 1,8-ND modification has no effect on perovskite band gap ($E_g = 1.55$ eV) judged from inset converted Tauc diagram. At the same time, the UV-vis absorption spectra of PbI_2 and PbI_2 with 1,8-ND films were also tested. As shown in Fig. S4, the appearance of different absorption edge indicates that 1,8-ND can combine with PbI_2 to form complexes, which may be related to the formation of low-dimensional perovskite [39].

Ultraviolet photoelectron spectroscopy (UPS) can characterize energy level arrangement of functional layers to further reveal carrier transport dynamics. By comparing and analyzing the cut-off edges in Fig. 2b, combined with the above E_g , schematic diagram (Fig. 2c) of energy level arrangement can be delineated [40]. Gradient arrangement of energy level structure between SnO_2 /perovskite/1,8-ND/spiro-OMeTAD can optimize charge transport, which is beneficial to the improvement of PSCs performance. The existence of the conduction band barrier at the 2D/3D junction can hinder the transport of electrons, effectively promoting the separation of carriers [41,42]. Moreover, Kelvin probe force microscopy (KPFM) was performed to characterize the distribution of surface potential on perovskite films. Comparison results in Fig. 2d show that the surface potential of 1,8-ND modified perovskite film is higher, which is the result of 1,8-ND molecule acting as a negative dipole for electron donating [43]. The changing trend of surface potential is consistent with UPS measurement, which is the result that the surface perovskite became more n-type, indicating that the hole trap between perovskite/HTL is effectively passivated [33]. Besides, stereogram and statistical curve results in Fig. S5 show that the surface potential of modified perovskite film becomes more homogeneous, which may be relevant to the optimization of defect at grain boundary.

Carrier dynamics of perovskite film can be effectively analyzed by measuring the fluorescence intensity and the decay condition caused by radiative recombination of photogenerated carriers after photoexcitation. The steady-state photoluminescence (PL) spectra of perovskite films is shown in Fig. 3a, the main PL peak is attribute to the target perovskite of $\text{FA}_{0.92}\text{MA}_{0.08}\text{PbI}_3$, and the shoulders on both sides may be caused by the incomplete transformation of FAPbI_3 . The 1,8-ND modified perovskite film exhibits much higher luminescence intensity than pristine film after photoexcitation at 534 nm, which is attributed to the significant reduction in the non-radiative recombination of charge carriers, exhibiting excellent defect passivation ability of 1,8-ND [44]. To further understand the effect of 1,8-ND on lifetime of photogenerated carriers, time-resolved photoluminescence (TRPL) decay tests were performed. As shown in Fig. 3b that the decay rate of fluorescence intensity of 1,8-ND modified perovskite film is apparently slowed down, indicating a prominent prolongation of lifetime in photogenerated carriers [45]. Table S1 shows the detailed parameters of decay curves after fitting and the carrier average TRPL life of 1,8-ND modified sample can reach 253.1 ns, which is observably longer than 90.6 ns of pristine sample. Extended decay lifetime means an increase in difficulty of carrier recombination, which leads to more carriers that can drift to the

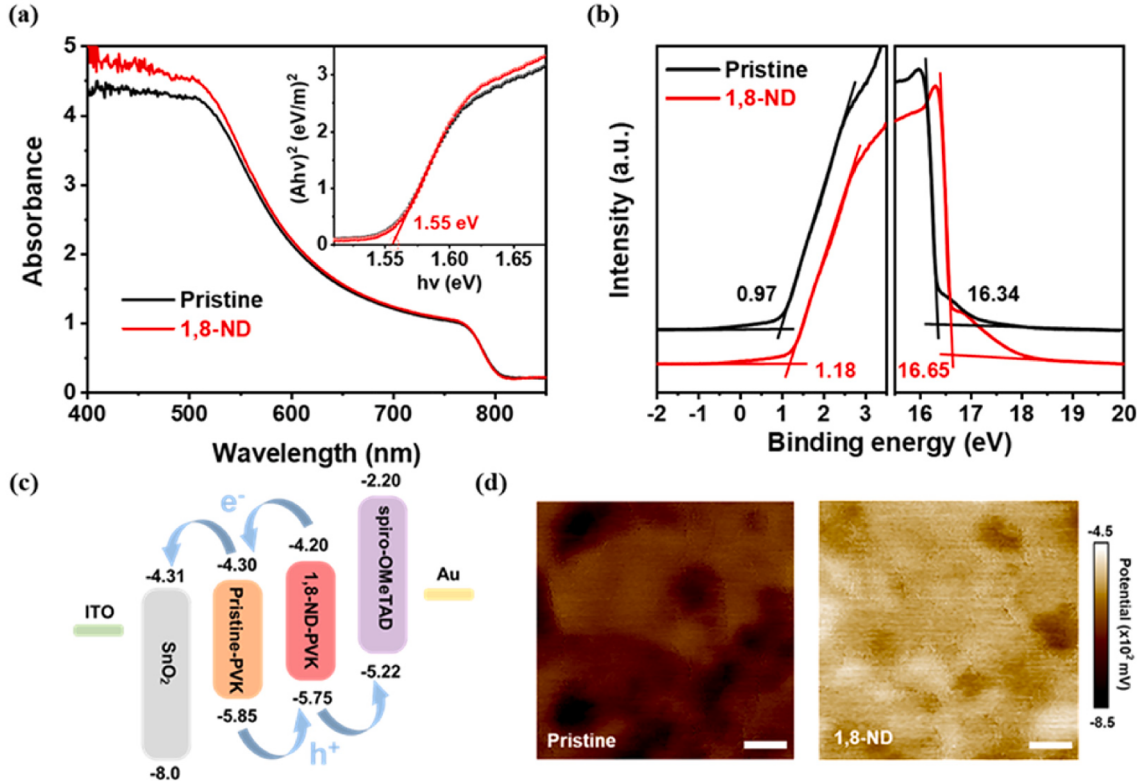


Fig. 2. (a) UV-vis spectra, (b) UPS spectra, (c) Schematic diagram of energy level arrangement of prepared PSCs (Pristine-PVK and 1,8-ND-PVK refers to the perovskite films without and with 1,8-ND modified) and (d) KPFM images (scale bar: 500 nm) of pristine and 1,8-ND modified perovskite films.

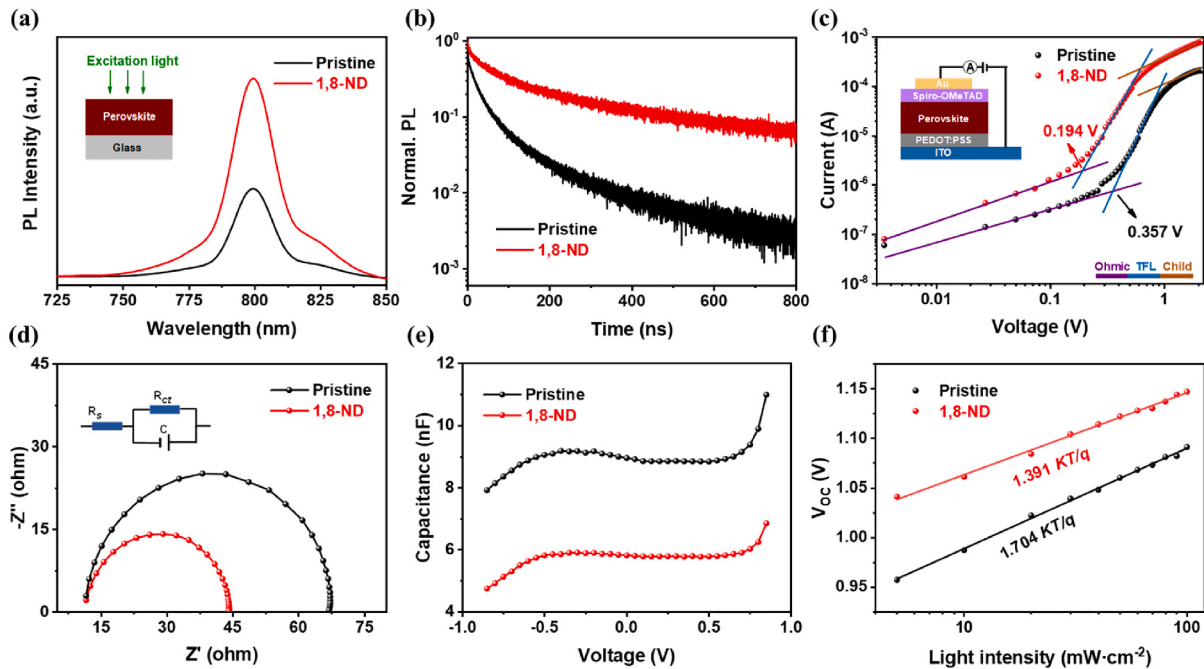


Fig. 3. (a) PL spectra, (b) TRPL spectra of pristine and 1,8-ND modified perovskite films. (c) dark I-V curves of prepared hole-only SCLC devices, (d) Nyquist plots under light condition, (e) C-V curves, (f) V_{oc} -light intensity curves of pristine and 1,8-ND modified PSCs.

surface of perovskite film, and ultimately achieves better optoelectronic properties [46]. PL mapping comparison shown in Fig. S6 exhibit the fluorescence intensity of 1,8-ND modified perovskite film on plane scale is improved due to the reduction of nonradiative recombination after defect passivation, consistent with PL results. Furthermore, optimized

film has more homogeneous luminescence property, which may ascribe to the passivation of defect at grain boundary by penetration of 1,8-ND, and it is beneficial for charge transfer as the energy loss during inter-domain transfer can be significantly reduced [32,34].

To further determine the effect of 1,8-ND on defect passivation, a

quantitative analysis of trap density (n_{trap}) was performed by hole-only transporting structure of ITO/PEDOT: PSS/perovskite/spiro-OMeTAD/Au by space charge limited current (SCLC) measurement. As shown in Fig. 3c, dark current–voltage (I - V) characteristic curves include three regions. As bias voltage increases, the trap is continuously filled until reaching trap-filled limit voltage (V_{TFL}) [47]. By comparison, V_{TFL} after 1,8-ND modification is 0.194 V, which is significantly lower than 0.357 V of pristine sample. In addition, the n_{trap} after 1,8-ND modification is calculated to be $1.10 \times 10^{15} \text{ cm}^{-3}$, lower than $2.03 \times 10^{15} \text{ cm}^{-3}$ of pristine sample. The significant decrease of n_{trap} is attributed to the excellent passivation of surface defect in perovskite films by 1,8-ND, which is beneficial to reduce nonradiative recombination of carriers and increase V_{OC} of PSCs.

The transport and recombination of carriers at surface are dominant factors affecting the performance of PSCs. Electrical impedance spectroscopy (EIS) can facilitate the analysis of surface charge transport, and its Nyquist plot under illumination is shown in Fig. 3d. Modified PSCs exhibited smaller charge-transfer resistance, indicating that 1,8-ND can contribute to charge transport and extraction [48]. In addition, the accumulation of carriers at surface can be explored by monitoring capacitance. As judged from capacitance-voltage (C - V) curves in Fig. 3e that with increasing bias voltage, 1,8-ND modified PSC has a smaller capacitance value, which means that the charge accumulation at surface between perovskite/HTL films is effectively reduced, consistent with the EIS result [49]. The mechanism of carrier recombination in PSCs can be more thoroughly revealed by measuring the dependence of V_{OC} on light intensity [50]. Fig. 3f indicate that the slope of 1,8-ND modification curve becomes moderate. By calculation, its ideality factor is dropped from $1.704 \text{ } K T/q$ to $1.391 \text{ } K T/q$ by the effective suppression of trap-assisted charge recombination.

To further explore the effect of 1,8-ND surface modification on optoelectronic property, n-i-p PSCs with ITO/SnO₂/perovskite/spiro-OMeTAD/Au were constructed. It can be seen from the cross-view SEM image (Fig. 4a) of prepared PSC that perovskite light-absorbing layer has a sufficient thickness, which ensures the effective absorption of incident light. Moreover, perovskite crystal particles exhibit a longitudinally penetrating structure, which facilitates the efficient separation and extraction of charges, and it is a prerequisite for PSCs with excellent performance. Current density–voltage (J - V) curves can further

demonstrate the effect of 1,8-ND on optoelectronic property. It can be judged from Fig. 4b and Table S2 that PSCs after 1,8-ND surface modification with different concentrations have distinct performance. Through continuous optimization, optimal modification concentration was locked at 4 mg mL⁻¹. Finally, it can be known based on Fig. 4c and Table S3 that 1,8-ND modified PSC achieved a champion PCE of 23.8% ($V_{\text{OC}} = 1.15 \text{ V}$, FF = 83.0%, $J_{\text{SC}} = 24.9 \text{ mA cm}^{-2}$) with negligible hysteresis compared to pristine the PSC with a PCE of 21.6% ($V_{\text{OC}} = 1.09 \text{ V}$, FF = 81.2%, $J_{\text{SC}} = 24.4 \text{ mA cm}^{-2}$) under reverse scan. The enhanced optoelectronic properties of PSCs are not only attributed to the effective passivation of surface defects, but also related to the existence of 2D/3D junctions that can control the carrier transport. To confirm the reproducibility of performance optimization by 1,8-ND modification, the key parameters of valid PSCs were counted. As shown in Fig. 4d and Fig. S7, the PCE improvement is mainly attributed to the extraordinary increase of V_{OC} , which is benefited from surface defect passivation by 1,8-ND to suppress the non-radiative recombination of carriers. Besides, J_{SC} and FF have also been improved. External quantum efficiency (EQE) curves can more accurately judge the improvement of J_{SC} . It can be seen from Fig. 4e that the integrated photocurrent density of 1,8-ND modified PSC reached 24.0 mA cm^{-2} , obviously higher than 23.5 mA cm^{-2} of pristine PSC. The results match well with J - V curves, further demonstrating the contribution of 1,8-ND to photocurrent output. Fig. 4f shows steady-state power output (SPO) of PSCs. Under continuous illumination, 1,8-ND modified PSCs exhibited a SPO of 22.8% (20.5% for pristine) at maximum power point (MPP) voltage, which is consistent with J - V curves, showing excellent and stable photoelectric conversion under continuous illumination.

Hydrophobic property of perovskite films can notably affect environmental stability of PSCs. In order to judge whether perovskite film after 1,8-ND surface modification has better hydrophobic property, a water-contact angle measurement was carried out. It can be determined from Fig. 5a that after 1,8-ND modification, the water-contact angles of perovskite films were increased from 51.0° to 70.9° , which is related to the hydrophobic ring of 1,8-ND molecule and the constructed quasi-2D perovskite [35]. To determine the improved environmental stability of perovskite, exposed films were tracked in air environment with a relative humidity of 30%. Fig. 5b shows that pristine perovskite film displayed obvious decomposition with pale yellow color after being placed

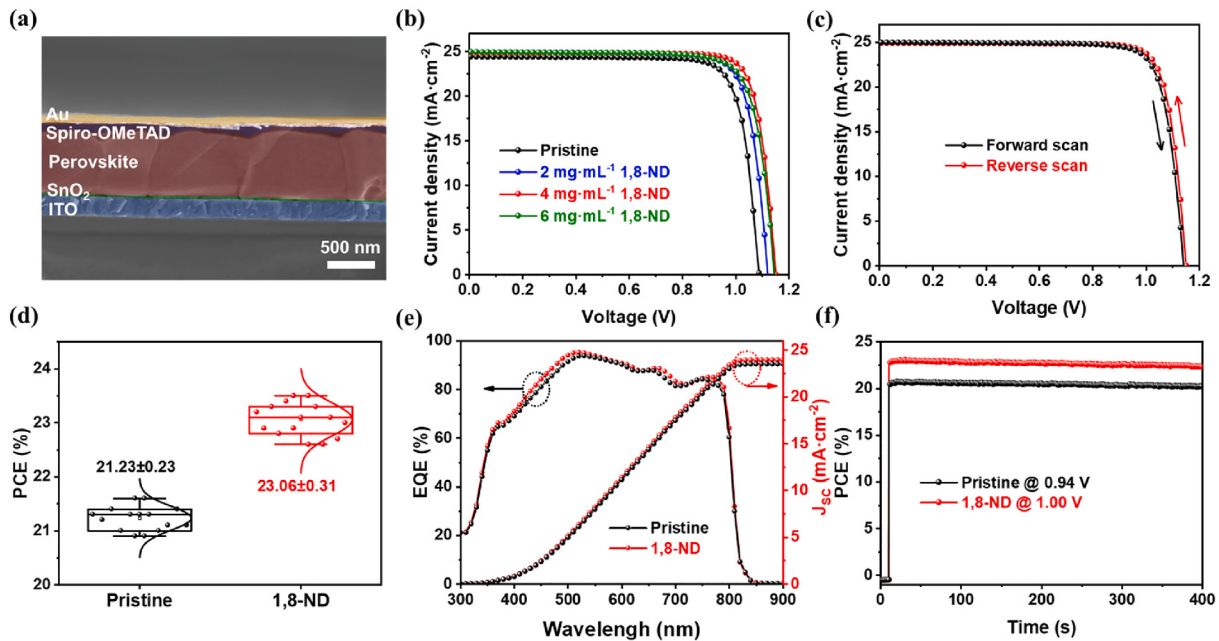


Fig. 4. (a) Cross-view SEM image of PSC. J-V curves of (b) PSCs modified with different concentrations of 1,8-ND and (c) PSCs modified by 4 mg mL⁻¹ 1,8-ND under forward and reverse scan. (d) Statistical distributions of PCE, (e) EQE curves and (f) SPO curves of pristine and 1,8-ND modified PSCs.

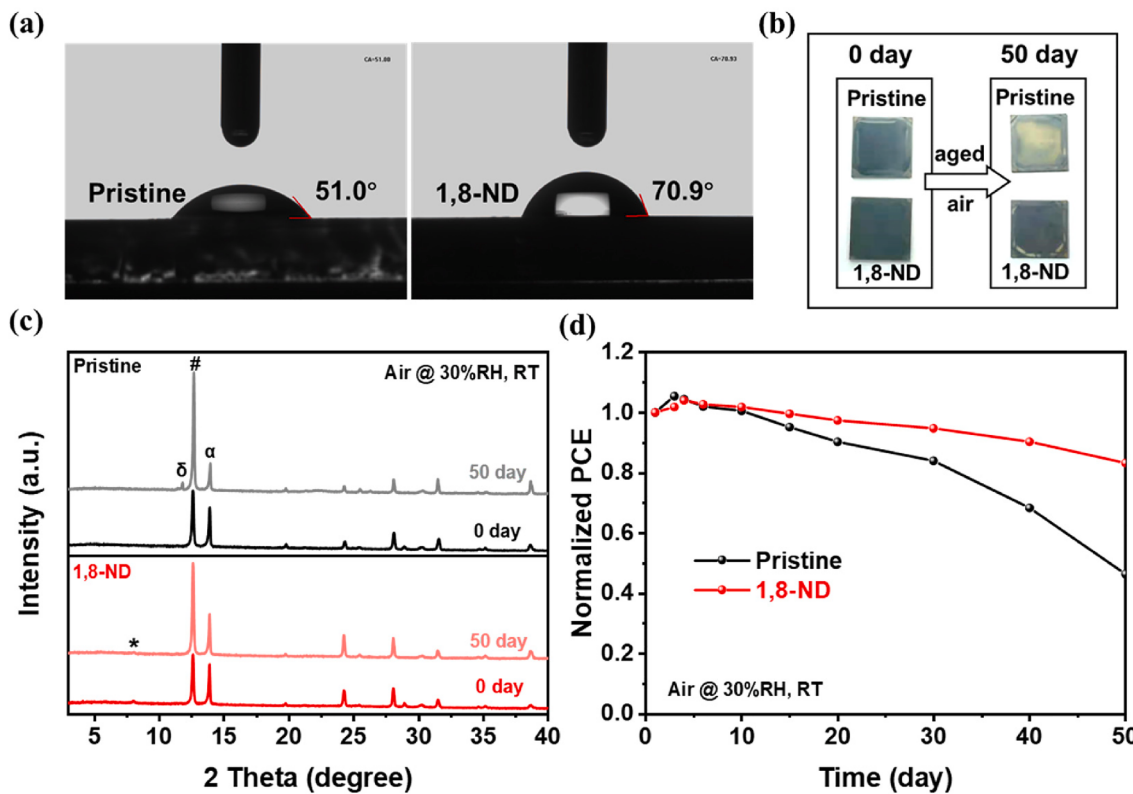


Fig. 5. (a) Water-contact angles, (b) initial and aged photos, (c) initial and aged XRD patterns of pristine and 1,8-ND modified perovskite films (α , δ , #, and * denote the peaks of α -FAPbI₃, δ -FAPbI₃, PbI₂, and quasi-2D perovskite). (d) PCE decline of prepared PSCs (RH and RT indicate relative humidity and room temperature).

in air for 50 days, while the optimized film displayed only less decomposition and no visible discoloration. The improved stability of perovskite films is not only attributed to the hydrophobic properties of 1,8-NDs and effective surface defect passivation, but also related to the better tolerance of lattice distortion in the constructed quasi-2D perovskite to suppress the phase transition of α -FAPbI₃ [23,51].

Moreover, XRD measurement was performed on aged perovskite films (Fig. 5c). Due to attack of moisture and instability of FA-based 3D perovskite, the diffraction peak of pristine α -FAPbI₃ located at $2\theta = 14.0^\circ$ decreased significantly after exploring in air for 50 days. Meanwhile, the diffraction peak of PbI₂ located at 12.7° was visibly enhanced, indicating that the pristine perovskite was overtly decomposed, which is consistent with the above results. Surprisingly, a diffraction peak of non-photoactive δ -FAPbI₃ at $2\theta = 11.8^\circ$ was also observed, indicating that pristine perovskite was accompanied by a phase transition of α -FAPbI₃ during decomposition [52]. However, the enhancement of PbI₂ diffraction peak was weaker for 1,8-ND modified perovskite, and δ -FAPbI₃ phase was not observed, indicating that the quasi-2D perovskite formed by 1,8-ND can inhibit the phase transition of α -FAPbI₃ by hindering the penetration of H₂O [51,52]. Finally, long-term PCE fluctuations of unencapsulated PSCs in air with 30% humidity were tracked. As shown in Fig. 5d, PCE has a slow climb in the initial stage of aging, which is related to downshift of the valence band after spiro-OMeTAD oxidation, and may also be related to defect self-healing of perovskite during aging [53]. Subsequently, PCE began to decline with varying magnitudes. After 50 days, pristine PSC declined significantly, leaving only 46.3% of initial PCE. However, the loss of PCE was significantly mitigated after 1,8-ND modification, and optimized PSC maintained 83.2% of initial PCE after aging, exhibiting excellent environmental stability. Moreover, MPP tracking was tested to assess the stability of operation stability of unencapsulated pristine and 1,8-ND modified PSCs, as shown in Fig. S8. 1,8-ND optimized 2D/3D PSC showed almost no decline after 100 h of MPP operation, while the pristine PSC had

dropped to 81% of the initial PCE, showing the outstanding continuous working stability of 1,8-ND optimized PSCs.

3. Conclusion

In summary, we remarkably passivated the surface defect on perovskite films based on 1,8-ND modification, and constructed 2D/3D perovskite with robust structure. The above results indicate that 1,8-ND molecule has electron-rich structure and can form effective coordination with Pb²⁺ ions as a Lewis base. Benefiting from the reduced non-radiative recombination and improved charge transport, the 1,8-ND optimized 2D/3D PSC obtained a champion PCE of 23.8% with negligible hysteresis and prominent steady-state performance. Based on the efficient passivation of defect and construction of quasi-2D perovskite, the hydrophobic property and phase stability of α -FAPbI₃ were significantly improved. Unencapsulated PSC retained 83.2% of initial PCE after 50 days of exposure in air with 30% humidity, showing excellent environmental stability. The dramatic improvement in performance confirms that the surface modification between perovskite/HTL films by 1,8-ND is a resultful strategy for fabricating efficient and stable PSCs.

Declaration of Competing Interest

The authors declare that they have no known competing financial interests or personal relationships that could have appeared to influence the work reported in this paper.

Data availability

Data will be made available on request.

Acknowledgments

The authors acknowledge the joint support from the National Natural Science Foundation of China (No. 51972123, U1705256 and 21771066). Thanks for the testing service provided by the IACHQU.

Appendix A. Supplementary data

Supplementary data to this article can be found online at <https://doi.org/10.1016/j.cej.2022.137806>.

References

- [1] G.E. Eperon, M.T. Hörantner, H.J. Snaith, Metal halide perovskite tandem and multiple-junction photovoltaics, *Nat. Rev. Chem.* 1 (12) (2017) 0095.
- [2] J. Huang, Y. Yuan, Y. Shao, Y. Yan, Understanding the physical properties of hybrid perovskites for photovoltaic applications, *Nat. Rev. Mater.* 2 (7) (2017) 17042.
- [3] S. Yang Woon, B.-W. Park, H. Jung Eui, J. Jeon Nam, C. Kim Young, U. Lee Dong, S. Shin Seong, J. Seo, K. Kim Eun, H. Noh Jun, I., Seok Sang, Iodide management in formamidinium-lead-halide-based perovskite layers for efficient solar cells, *Science* 356 (6345) (2017) 1376–1379.
- [4] A. Kojima, K. Teshima, Y. Shirai, T. Miyasaka, Organometal halide perovskites as visible-light sensitizers for photovoltaic cells, *J. Am. Chem. Soc.* 131 (17) (2009) 6050–6051.
- [5] NREL. Best Research Cell Efficiency Chart. <https://www.nrel.gov/pv/assets/pdfs/best-research-cell-efficiencies-rev220126.pdf>.
- [6] Y. Tu, J. Wu, G. Xu, X. Yang, R. Cai, Q. Gong, R. Zhu, W. Huang, Perovskite solar cells for space applications: progress and challenges, *Adv. Mater.* 33 (21) (2021) 2006545.
- [7] H. Lu, Y. Liu, P. Ahlawat, A. Mishra, R. Tress Wolfgang, T. Eickemeyer Felix, Y. Yang, F. Fu, Z. Wang, E. Avalos Claudia, I. Carlsen Brian, A. Agarwalla, X. Zhang, X. Li, Y. Zhao, M. Zakeeruddin Shaik, L. Emsley, U. Rothlisberger, L. Zheng, A. Hagfeldt, M. Grätzel, Vapor-assisted deposition of highly efficient, stable black-phase FAPbI₃ perovskite solar cells, *Science* 370 (6512) (2020) eabb8985.
- [8] G. Kim, H. Min, S. Lee Kyoung, Y. Lee Do, M. Yoon So, I., Seok Sang, Impact of strain relaxation on performance of α -formamidinium lead iodide perovskite solar cells, *Science* 370 (2020) 108–112.
- [9] Q. Jiang, Y. Zhao, X. Zhang, X. Yang, Y. Chen, Z. Chu, Q. Ye, X. Li, Z. Yin, J. You, Surface passivation of perovskite film for efficient solar cells, *Nat. Photonics* 13 (7) (2019) 460–466.
- [10] M. Kim, G. Kim, T. Lee, I. Choi, H. Choi, Y. Jo, Y. Yoon, J. Kim, J. Lee, D. Huh, H. Lee, S. Kwak, J. Kim, D.S. Kim, Methylammonium chloride induces intermediate phase stabilization for efficient perovskite solar cells, *Joule* 3 (9) (2019) 2179–2192.
- [11] M. Wang, S. Tan, Y. Zhao, P. Zhu, Y. Yin, Y. Feng, T. Huang, J. Xue, R. Wang, G. Han, H. Jung, J. Bian, J. Lee, Y. Yang, Stable and efficient methylammonium-cesium-, and bromide-free perovskite solar cells by in-situ interlayer formation, *Adv. Funct. Mater.* 31 (7) (2021) 2007520.
- [12] W. Wu, P. Rudd, Z. Ni, C. Van Brackle, H. Wei, Q. Wang, B. Ecker, Y. Gao, J. Huang, Reducing surface halide deficiency for efficient and stable iodide-based perovskite solar cells, *J. Am. Chem. Soc.* 142 (8) (2020) 3989–3996.
- [13] W. Zhao, P. Guo, J. Su, Z. Fang, N. Jia, C. Liu, L. Ye, Q. Ye, J. Chang, H. Wang, Synchronous passivation of defects with low formation energies via terdentate anchoring enabling high performance perovskite solar cells with efficiency over 24%, *Adv. Funct. Mater. Early View* (2022) 2200534, <https://doi.org/10.1002/adfm.202200534>.
- [14] J. Wu, J. Shi, Y. Li, H. Li, H. Wu, Y. Luo, D. Li, Q. Meng, Quantifying the interface defect for the stability origin of perovskite solar cells, *Adv. Energy Mater.* 9 (37) (2019) 1901352.
- [15] G. Li, J. Wu, J. Song, C. Meng, Z. Song, X. Wang, X. Liu, Y. Yang, D. Wang, Z. Lan, Excellent quinoline additive in perovskite toward to efficient and stable perovskite solar cells, *J. Power Sources* 481 (2021), 228857.
- [16] T. Zhou, H. Lai, T. Liu, D. Lu, X. Wan, X. Zhang, Y. Liu, Y. Chen, Highly efficient and stable solar cells based on crystalline oriented 2D/3D hybrid perovskite, *Adv. Mater.* 31 (32) (2019) 1901242.
- [17] Z. Ni, C. Bao, Y. Liu, Q. Jiang, W.-Q. Wu, S. Chen, X. Dai, B. Chen, B. Hartweg, Z. Yu, Z. Holman, J. Huang, Resolving spatial and energetic distributions of trap states in metal halide perovskite solar cells, *Science* 367 (6484) (2020) 1352–1358.
- [18] F. Gao, Y. Zhao, X. Zhang, J. You, Recent progresses on defect passivation toward efficient perovskite solar cells, *Adv. Energy Mater.* 10 (13) (2020) 1902650.
- [19] C. Deng, J. Wu, Y. Du, Q. Chen, Z. Song, G. Li, X. Wang, J. Lin, W. Sun, M. Huang, Y. Huang, P. Gao, Z. Lan, Surface reconstruction and in situ formation of 2D layer for efficient and stable 2D/3D perovskite solar cells, *Small Methods* 5 (12) (2021) 2101000.
- [20] Q. Zhang, J. Duan, Q. Guo, J. Zhang, D. Zheng, F. Yi, X. Yang, Y. Duan, Q. Tang, Thermal-triggered dynamic disulfide bond self-heals inorganic perovskite solar cells, *Angew. Chem., Int. Ed.* 61 (8) (2022) e202116632.
- [21] M. Wang, Y. Zhao, X. Jiang, Y. Yin, I. Yavuz, P. Zhu, A. Zhang, G.S. Han, H.S. Jung, Y. Zhou, W. Yang, J. Bian, S. Jin, J.-W. Lee, Y. Yang, Rational selection of the polymeric structure for interface engineering of perovskite solar cells, *Joule* 6 (5) (2022) 1032–1048.
- [22] Y. Chen, Y. Sun, J. Peng, J. Tang, K. Zheng, Z. Liang, 2D Ruddlesden-Popper perovskites for optoelectronics, *Adv. Mater.* 30 (2) (2018) 1703487.
- [23] J.-W. Lee, Z. Dai, T.-H. Han, C. Choi, S.-Y. Chang, S.-J. Lee, N. De Marco, H. Zhao, P. Sun, Y. Huang, Y. Yang, 2D perovskite stabilized phase-pure formamidinium perovskite solar cells, *Nat. Commun.* 9 (1) (2018) 3021.
- [24] P. Liu, N. Han, W. Wang, R. Ran, W. Zhou, Z. Shao, High-quality Ruddlesden-Popper perovskite film formation for high-performance perovskite solar cells, *Adv. Mater.* 33 (10) (2021) 2002582.
- [25] R. Azmi, E. Ugur, A. Seitkhan, F. Aljamaan, S. Subbiah Anand, J. Liu, T. Harrison George, I. Nugraha Mohamad, K. Eswaran Mathan, M. Babics, Y. Chen, F. Xu, G. Allen Thomas, U. Rehman Atteq, C.-L. Wang, D. Anthopoulos Thomas, U. Schwingenschlögl, M. De Bastiani, E. Aydin, S. De Wolf, Damp heat-stable perovskite solar cells with tailored-dimensionality 2D/3D heterojunctions, *Science* 376 (2022) 73–77.
- [26] G. Li, J. Song, J. Wu, Z. Song, X. Wang, W. Sun, L. Fan, J. Lin, M. Huang, Z. Lan, P. Gao, Efficient and stable 2D@3D/2D perovskite solar cells based on dual optimization of grain boundary and interface, *ACS Energy Lett.* 6 (10) (2021) 3614–3623.
- [27] M. Jung, S.-G. Ji, G. Kim, S.I. Seok, Perovskite precursor solution chemistry: from fundamentals to photovoltaic applications, *Chem. Soc. Rev.* 48 (7) (2019) 2011–2038.
- [28] W.-Q. Wu, Z. Yang, N. Rudd Peter, Y. Shao, X. Dai, H. Wei, J. Zhao, Y. Fang, Q. Wang, Y. Liu, Y. Deng, X. Xiao, Y. Feng, J. Huang, Bilateral alkylamine for suppressing charge recombination and improving stability in blade-coated perovskite solar cells, *Sci. Adv.* 5 (3) (2019) eaav8925.
- [29] J. Wang, L. Liu, S. Chen, G. Ran, W. Zhang, M. Zhao, C. Zhao, F. Lu, T. Jiu, Y. Li, Growth of 2D passivation layer in FAPbI₃ perovskite solar cells for high open-circuit voltage, *Nano Today* 42 (2022), 101357.
- [30] D.P. Asanin, S. Skaro, F. Bogojevic, T.P. Perdih, D. Andrejević, I. Milivojevic, J. Aleksić, B.D. Nikodinovic-Runic, I. Glisic, M.I. Turel, Djuran Structural characterization, antimicrobial activity and BSA/DNA binding affinity of new silver(I) complexes with thianthrene and 1,8-naphthyridine, *Molecules* 26 (7) (2021) 1871.
- [31] Q. Chen, K. Deng, Y. Shen, L. Li, Stable one dimensional (1D)/three dimensional (3D) perovskite solar cell with an efficiency exceeding 23%, *InfoMat* 4 (5) (2022) e12303.
- [32] J. Hu, C. Wang, S. Qiu, Y. Zhao, E. Gu, L. Zeng, Y. Yang, C. Li, X. Liu, K. Forberich, C.J. Brabec, M.K. Nazeeruddin, Y. Mai, F. Guo, Spontaneously self-assembly of a 2D/3D heterostructure enhances the efficiency and stability in printed perovskite solar cells, *Adv. Energy Mater.* 10 (2020) 2000173.
- [33] X. Yang, Y. Fu, R. Su, Y. Zheng, Y. Zhang, W. Yang, M. Yu, P. Chen, Y. Wang, J. Wu, D. Luo, Y. Tu, L. Zhao, Q. Gong, R. Zhu, Superior carrier lifetimes exceeding 6 μ s in polycrystalline halide perovskites, *Adv. Mater.* 32 (39) (2020) 2002585.
- [34] F. Li, X. Deng, F. Qi, Z. Li, D. Liu, D. Shen, M. Qin, S. Wu, F. Lin, S.-H. Jang, J. Zhang, X. Lu, D. Lei, C.-S. Lee, Z. Zhu, A.K.Y. Jen, Regulating surface termination for efficient inverted perovskite solar cells with greater than 23% efficiency, *J. Am. Chem. Soc.* 142 (47) (2020) 20134–20142.
- [35] G. Wu, R. Liang, M. Ge, G. Sun, Y. Zhang, G. Xing, Surface passivation using 2D perovskites toward efficient and stable perovskite solar cells, *Adv. Mater.* 34 (8) (2022) 2105635.
- [36] Y. Du, J. Wu, X. Zhang, Q. Zhu, M. Zhang, X. Liu, Y. Zou, S. Wang, W. Sun, Surface passivation using pyridinium iodide for highly efficient planar perovskite solar cells, *J. Energy Chem.* 52 (2021) 84–91.
- [37] P. Huang, S. Kazim, M. Wang, S. Ahmad, Toward phase stability: Dion-Jacobson layered perovskite for solar cells, *ACS Energy Lett.* 4 (12) (2019) 2960–2974.
- [38] P. Chen, Y. Bai, S. Wang, M. Lyu, J.-H. Yun, L. Wang, In situ growth of 2D perovskite capping layer for stable and efficient perovskite solar cells, *Adv. Funct. Mater.* 28 (17) (2018) 1706923.
- [39] Y. Zhan, F. Yang, W. Chen, H. Chen, Y. Shen, Y. Li, Y. Li, Elastic lattice and excess charge carrier manipulation in 1D–3D perovskite solar cells for exceptionally long-term operational stability, *Adv. Mater.* 33 (48) (2021) 2105170.
- [40] G. Li, J. Song, C. Meng, D. Wang, Z. Du, W. Sun, J. Wu, Z. Lan, Single source, surfactant-free, and one-step solvothermal route synthesized TiO₂ microspheres for highly efficient mesoscopic perovskite solar cells, *Sol. RRL* 4 (12) (2020) 2000519.
- [41] Z. Wang, Q. Lin, F.P. Chmiel, N. Sakai, L.M. Herz, H.J. Snaith, Efficient ambient-air-stable solar cells with 2D–3D heterostructured butylammonium-caesium-formamidinium lead halide perovskites, *Nat. Energy* 2 (9) (2017) 17135.
- [42] H. Chen, S. Teale, B. Chen, Y. Hou, L. Grater, T. Zhu, K. Bertens, S. Park, H. Atapattu, Y. Gao, M. Wei, A. Johnston, Q. Zhou, K. Xu, D. Yu, C. Han, T. Cui, E. Jung, C. Zhou, W. Zhou, A. Propp, S. Hoogland, F. Laquai, T. Filletier, K. Graham, Z. Ning, E. Sargent, Quantum-size-tuned heterostructures enable efficient and stable inverted perovskite solar cells, *Nat. Photonics* 16 (5) (2022) 352–358.
- [43] L. Canil, T. Cramer, B. Fraboni, D. Ricciarelli, D. Meggiolaro, A. Singh, M. Liu, M. Rusu, C.M. Wolff, N. Phung, Q. Wang, D. Neher, T. Unold, P. Vivo, A. Gagliardi, F. De Angelis, A. Abate, Tuning halide perovskite energy levels, *Energy Environ. Sci.* 14 (3) (2021) 1429–1438.
- [44] R. Wang, J. Xue, K.-L. Wang, Z.-K. Wang, Y. Luo, D. Fenning, G. Xu, S. Nuryyeva, T. Huang, Y. Zhao, L. Yang Jonathan, J. Zhu, M. Wang, S. Tan, I. Yavuz, N. Houk Kendall, Y. Yang, Constructive molecular configurations for surface-defect passivation of perovskite photovoltaics, *Science* 366 (6472) (2019) 1509–1513.
- [45] Q. Han, S.-H. Bae, P. Sun, Y.-T. Hsieh, Y. Yang, Y.S. Rim, H. Zhao, Q. Chen, W. Shi, G. Li, Y. Yang, Single crystal formamidinium lead iodide (FAPbI₃): insight into the structural, optical, and electrical properties, *Adv. Mater.* 28 (11) (2016) 2253–2258.

- [46] J. Song, H. Xie, E.L. Lim, Y. Li, T. Kong, Y. Zhang, X. Zhou, C. Duan, D. Bi, Multistrategy toward highly efficient and stable CsPbI₂Br Perovskite Solar Cells Based on Dopant-Free Poly(3-Hexylthiophene), *Sol. RRL* 6 (4) (2021) 2100880.
- [47] D.-Y. Son, S.-G. Kim, J.-Y. Seo, S.-H. Lee, H. Shin, D. Lee, N.-G. Park, Universal approach toward hysteresis-free perovskite solar cell via defect engineering, *J. Am. Chem. Soc.* 140 (4) (2018) 1358–1364.
- [48] Y. Xu, G. Li, R. Li, Y. Jing, H. Zhang, X. Wang, Z. Du, J. Wu, Z. Lan, PbS/CdS heterojunction thin layer affords high-performance carbon-based all-inorganic solar cells, *Nano Energy* 95 (2022), 106973.
- [49] Y. Li, Y. Zhao, Q. Chen, Y. Yang, Y. Liu, Z. Hong, Z. Liu, Y.-T. Hsieh, L. Meng, Y. Li, Y. Yang, Multifunctional fullerene derivative for interface engineering in perovskite solar cells, *J. Am. Chem. Soc.* 137 (49) (2015) 15540–15547.
- [50] Y. Cai, J. Cui, M. Chen, M. Zhang, Y. Han, F. Qian, H. Zhao, S. Yang, Z. Yang, H. Bian, T. Wang, K. Guo, M. Cai, S. Dai, Z. Liu, S. Liu, Multifunctional enhancement for highly stable and efficient perovskite solar cells, *Adv. Funct. Mater.* 31 (7) (2021) 2005776.
- [51] A. Alanazi, D. Kubicki, D. Prochowicz, E. Alharbi, M. Bouduban, F. Jahanbakhshi, M. Mladenović, J. Milić, F. Giordano, D. Ren, A. Alyamani, H. Albritthen, A. Albadri, M. Alotaibi, J. Moser, S. Zakeeruddin, U. Rothlisberger, L. Emsley, M. Gratzel, Atomic-level microstructure of efficient formamidinium-based perovskite solar cells stabilized by 5-ammonium valeric acid iodide revealed by multinuclear and two-dimensional solid-state NMR, *J. Am. Chem. Soc.* 141 (2019) 17659–17669.
- [52] A. Binek, F.C. Hanusch, P. Docampo, T. Bein, Stabilization of the trigonal high-temperature phase of formamidinium lead iodide, *J. Phys. Chem. Lett.* 6 (7) (2015) 1249–1253.
- [53] Y. Cho, H.D. Kim, J. Zheng, J. Bing, Y. Li, M. Zhang, M.A. Green, A. Wakamiya, S. Huang, H. Ohkita, A.W.Y. Ho-Baillie, Elucidating mechanisms behind ambient storage-induced efficiency improvements in perovskite solar cells, *ACS Energy Lett.* 6 (3) (2021) 925–933.